

ARTICLE

Fracture prediction based on W-transform inversion spectral decomposition

Xiuwei Wang^{1,2,3}, Ying Jia^{2,3}, Xilin Qin^{1*} , Jun Wang^{2,3}, and Yinglong Li¹ ¹Key Laboratory of Oil and Gas Resources and Exploration Technology, Ministry of Education, Yangtze University, Wuhan, Hubei, China²Research Institute of Exploration and Development, PetroChina Huabei Oilfield Company, Renqiu, Hebei, China³CNPC International Chad Company, Beijing, China

Abstract

Conventional ant-tracking technology is effective for fault identification, but its application is constrained by sensitivity to data quality and inadequate continuity of fault tracking results. This limitation creates an urgent need for optimization. To address this issue, this study proposes a frequency-divided ant-tracking method based on W-transform inversion spectral decomposition (WT-ISD) to improve the accuracy of fracture prediction in complex structural areas. By integrating the flexible time–frequency localization of the W-transform with sparse inversion theory, this method markedly improves the resolution and focusing performance of time–frequency spectra. This is achieved through the construction of an overcomplete dictionary and the imposition of L1 norm constraints. The proposed method not only provides a novel high-resolution time–frequency analysis tool for seismic signal processing but also establishes a theoretical basis for subsequent fine geological interpretation via its frequency-divided processing workflow. Taking the Raphia S Block in the Bongor Basin as a case study, this research first adopts WT-ISD to obtain high-resolution spectral decomposition results, generating single-frequency data volumes corresponding to different frequency components. Subsequently, structural smoothing filtering and boundary enhancement processing are applied to highlight discontinuity information. Then, the ant-tracking algorithm is introduced, combined with regional structural attitude constraints, to realize the identification of multi-scale fractures. Finally, red–green–blue attribute fusion technology is used to integrate responses from different frequencies and construct a fault distribution model. Practical application results indicate that this method not only improves the accuracy and spatial continuity of fracture prediction but also enhances its anti-noise capability. In particular, it exhibits excellent identification performance for large-, medium-, and small-scale fractures corresponding to 20 Hz, 35 Hz, and 50 Hz, respectively. This study verifies that the proposed method can provide reliable technical support for multi-scale fracture detection in complex structural areas and demonstrates important application value for fracture prediction in oil and gas exploration.

***Corresponding author:**

Xilin Qin (qxl@yangtzeu.edu.cn)

Citation: Wang X, Jia Y, Qin X, Wang J, Li Y. Fracture prediction based on W-transform inversion spectral decomposition. *J Seismic Explor.* 2026;35(2):025010140. doi: 10.36922/JSE025010140

Received: December 30, 2025**Revised:** February 6, 2026**Accepted:** March 2, 2026**Published online:** April 15, 2026

Copyright: © 2026 Author(s). This is an Open-Access article distributed under the terms of the Creative Commons Attribution License, permitting distribution, and reproduction in any medium, provided the original work is properly cited.

Publisher's Note: AccScience Publishing remains neutral with regard to jurisdictional claims in published maps and institutional affiliations.

Keywords: Frequency-divided ant-tracking; Fracture prediction; W-transform; Inversion spectral decomposition; Red–green–blue attribute fusion

1. Introduction

Fractures serve as crucial reservoir spaces and seepage channels in oil and gas reservoirs. Their spatial distribution characteristics directly affect oil and gas accumulation and productivity, making them a key geological basis for formulating exploration and development plans.¹ Based on scale and genesis, fracture systems are generally classified into three categories. Large-scale faults and fault zones extend several kilometers and are typically formed by regional tectonic movements. Medium-scale structural fractures and fracture zones span tens to hundreds of meters and are mostly related to local structural deformation. Small-scale fractures such as microfractures and joints extend several meters to more than ten meters and are mainly controlled by diagenesis or local stress.² Different-scale fractures contribute differently to reservoir storage and seepage. Thus, the effective identification and detailed characterization of multi-scale fractures have long been a core challenge in the field of oil and gas geophysics.

Current fracture prediction methods are mainly divided into pre-stack and post-stack categories. Pre-stack methods, such as azimuthal anisotropy inversion, can evaluate fracture orientation and density using the directionality of seismic waves. Post-stack methods primarily rely on seismic attribute analysis, including discontinuity detection technologies such as coherence cubes, curvature attributes, and ant-tracking.^{3,4} However, due to the multi-scale nature and genetic complexity of fracture systems, a single technology often fails to effectively characterize fracture networks of different scales simultaneously. Prediction results are usually a mixed reflection of multi-scale geophysical responses. This highlights the need for methods capable of separating and characterizing multi-scale fractures to improve the reliability and practicality of fracture prediction.

Seismic signals exhibit typical non-stationary characteristics. The traditional Fourier transform can only reflect the global frequency distribution of signals and cannot effectively characterize their local time-frequency evolution features. This limitation severely restricts the accurate extraction of detailed subsurface geological information. To address this issue, time-frequency analysis techniques have been widely applied in seismic data processing and interpretation, and are mainly categorized into linear and nonlinear types. Linear time-frequency analyses include the short-time Fourier transform (STFT),⁵ wavelet transform,⁶ and S-transform (ST).⁷ Nonlinear time-frequency analyses encompass the Wigner-Ville distribution,⁸ matching pursuit,⁹ and frequency reassignment.¹⁰ These techniques offer solid technical support for improving the identification accuracy

of thin layers and complex geological bodies.

Specifically, the spectral decomposition method proposed by Partyka *et al.*¹¹ has successfully revealed subtle geological details that are indistinguishable in conventional broadband data by generating discrete single-frequency data volumes. Furthermore, Zeng *et al.*¹² confirmed that single-frequency data volumes possess unique advantages in characterizing the spatial distribution of geological anomalies, providing a new technical approach for the detailed characterization of oil and gas reservoirs.

Nevertheless, traditional linear time-frequency analyses are constrained by the inherent properties of window functions, generally suffering from insufficient resolution in low-frequency regions. This directly leads to inadequate accuracy in identifying key geological features of oil and gas reservoirs, which has become a core bottleneck restricting the efficiency of oil and gas exploration. To address this technical challenge, Wang¹³ proposed the W-transform (WT). Its core innovation lies in optimizing the window kernel function of traditional linear transforms using the instantaneous dominant frequency of seismic data and in constructing an improved dominant frequency estimation formula. These improvements not only overcome the theoretical limitations of traditional linear time-frequency analysis but also significantly enhance its practical application value in production scenarios such as reservoir description.

Since the proposal of the WT, researchers have conducted extensive targeted studies on the optimization and upgrading of its window kernel function, leading to the development of several modified versions with important application value. Li *et al.*¹⁴ conducted an in-depth analysis of the mathematical model of the conventional WT and discovered a derivative singularity near the dominant frequency, which causes distortion in the extraction of time-frequency features in the dominant frequency region. To resolve this defect, they reconstructed the window kernel function into a polynomial form and proposed the generalized WT, effectively improving the time-frequency resolution of the WT near the dominant frequency.

The three-parameter WT proposed by Chen *et al.*¹⁵ shares the same design philosophy as the generalized WT. By introducing three auxiliary control parameters, it achieves precise adaptation of the time-frequency resolution of the smoothed Gaussian window, further enhancing the characterization accuracy of the time-frequency spectra of seismic data. Luo *et al.*¹⁶ integrated the core idea of the synchrosqueezing transform into the WT framework and proposed the synchrosqueezing WT. This significantly improves the performance of the WT in detecting small-scale geological bodies such as thin layers

and channels, offering more powerful technical support for the detailed characterization of small-scale geological bodies.

In addition, the normalized WT proposed by Chen *et al.*¹⁷ effectively solves the spectral energy splitting problem of the WT in broadband seismic signal analysis. It achieves this by normalizing the standard deviation along the time-varying dominant frequency, significantly improving the time–frequency resolution and reservoir interpretation accuracy. These modified versions continuously enrich and improve the theoretical system and application scenarios of the WT, providing more efficient technical approaches for oil and gas exploration under complex geological conditions.

Ant-tracking technology provides another effective approach for fracture detection. Originating from the ant colony algorithm proposed by Dorigo *et al.*¹⁸, its global optimization characteristics lay a theoretical foundation for seismic discontinuity identification. In recent years, multi-scale ant-tracking technology has promoted the refined development of fracture characterization. For example, Yuan and Simons¹⁹ proposed a multi-scale full-waveform inversion method based on the wavelet transform. It achieves step-by-step inversion from long wavelengths to seismic phase details through wavelet decomposition, significantly improving convergence and stability. Wen *et al.*²⁰ proposed and applied a fracture identification method based on the multi-channel synchrosqueezing generalized ST. By leveraging its high time–frequency focusing capability, it maximizes the retention of fracture information and reduces errors in time–frequency conversion, realizing multi-scale fault characterization.

Moreover, Liu *et al.*²¹ proposed a novel time–frequency analysis method called the synchrosqueezing extraction transform. It aims to improve the concentration of the time–frequency representation of non-stationary vibration signals, effectively extracting time-varying information from the signals and obtaining clearer time–frequency representations. Xie *et al.* established a frequency-divided optimized ant-tracking workflow.²² Through multi-frequency band collaborative processing, it significantly enhances the continuity of fracture prediction and the identification ability of small-scale fractures.

Meanwhile, time–frequency analysis methods are continuously evolving. For instance, the improved synchrosqueezing transform proposed by Yu *et al.*,²³ the time-synchroextracting generalized ST extraction method established by Zhang *et al.*,²⁴ the matched demodulation synchrosqueezing ST designed by Wang *et al.*,²⁵ and the short-time fractional Fourier transform spectrum proposed by Tian²⁶ have all improved time–frequency

focusing and reservoir characterization accuracy from different perspectives.

However, existing methods still have limitations in separating multi-scale fracture responses. How to effectively perform high-resolution time–frequency analysis for fracture detection algorithms remains a topic worthy of further investigation. Therefore, the present study integrates the advantages of sparse inversion and the WT to construct a novel high-resolution time–frequency analysis method—WT inversion spectral decomposition (WT-ISD). It also combines WT-ISD with ant-tracking technology to propose a multi-scale fracture prediction method based on frequency-divided processing. This method aims to obtain single-frequency data volumes that are sensitive to fractures of specific scales through spectral decomposition. Additionally, the study uses ant-tracking under regional structural constraints to realize the separation and detection of fractures at different scales. Finally, it constructs a complete fault distribution model through red–green–blue (RGB) attribute fusion technology. This study verifies the effectiveness of the method in improving fracture prediction accuracy, continuity, and anti-noise capability using data from an actual study area, providing reliable technical support for multi-scale fracture characterization in complex structural areas.

2. Methodology

The frequency-divided ant-tracking method based on WT-ISD offers distinct advantages in fracture interpretation, with the specific workflow illustrated in [Figure 1](#). Based on post-stack three-dimensional (3D) seismic data, spectral analysis of the seismic data was first conducted to clarify the dominant frequency band range of the dataset. Subsequently, by virtue of the high-precision time–frequency analysis method WT-ISD, 12 single-frequency seismic data volumes with different dominant frequencies were extracted within the effective frequency band. These 12 single-frequency volumes were then preprocessed to suppress noise and improve the signal-to-noise ratio, aiming to enhance the discontinuity characteristics in the data. Then, an in-depth analysis was conducted on the detection response differences of the post-stack seismic variance attribute among single-frequency volumes of different frequency bands.

Fracture information corresponding to each dominant frequency was extracted through discontinuity detection, and through comprehensive comparison, three single-frequency attribute data volumes from different frequency bands that best highlight feature characteristics at different scales and are suitable for ant-tracking-based fracture

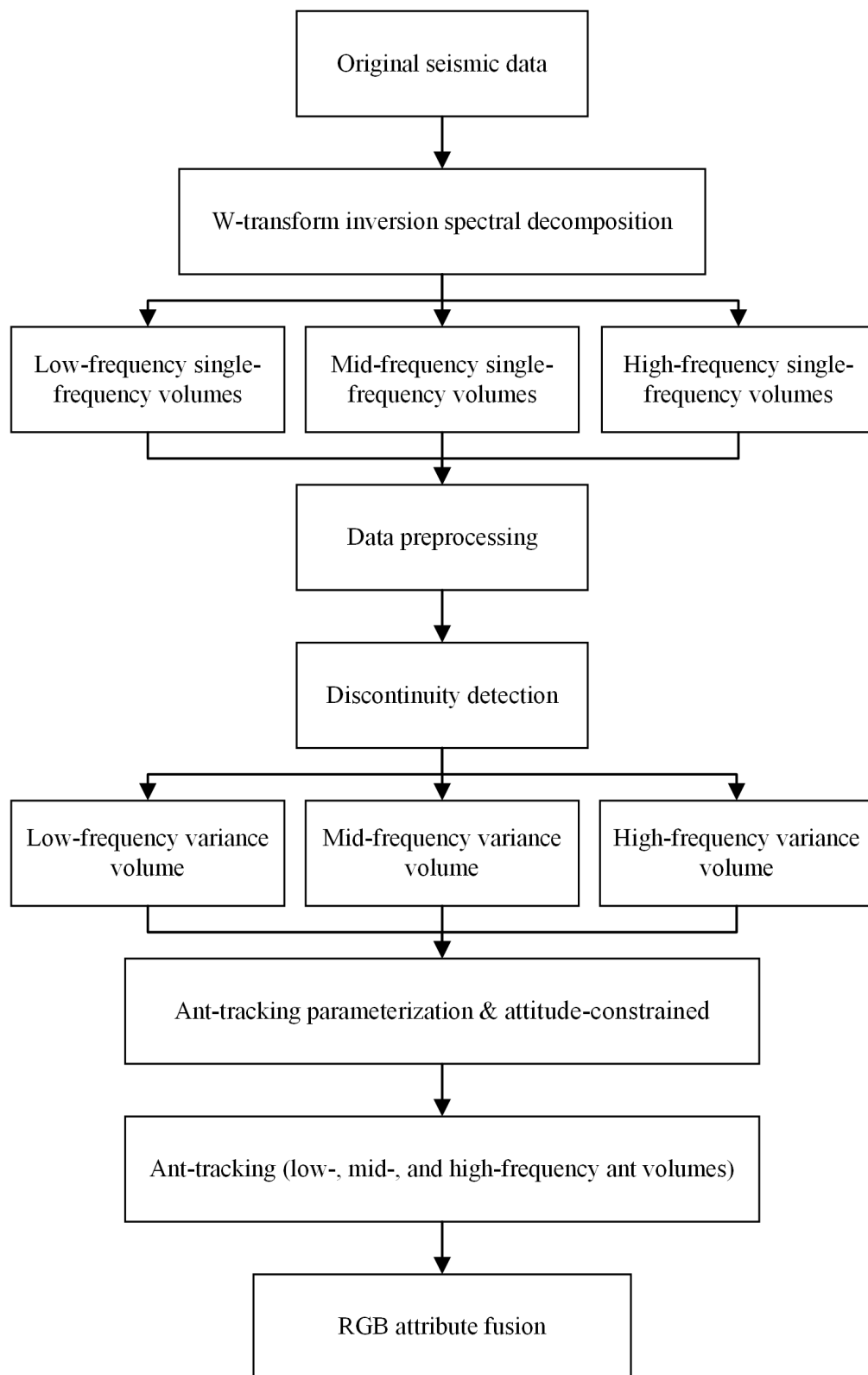


Figure 1. Workflow of frequency-divided ant-tracking
Abbreviation: RGB: Red-green-blue.

detection were selected. Finally, when applying the ant-tracking method to conduct fracture tracing on the optimally selected single-frequency variance data volumes that can characterize fractures at three different scales, attitude control must be implemented in combination with the regional structural background to ensure that the tracing results are consistent with geological reality, thereby realizing the effective prediction and detailed characterization of fractures of different scales.

Ultimately, results were generated and verified through attribute fusion. The RGB attribute fusion technology integrates single-frequency data volumes with different frequency components, enabling comprehensive consideration of the multi-scale development characteristics of fractures under each frequency band and effectively improving prediction accuracy. Through this workflow, the frequency-divided ant-tracking fracture prediction method based on WT-ISD can significantly enhance the accuracy and reliability of fault interpretation.

2.1. W-transform inversion spectral decomposition

Time-frequency analysis technology is a class of mathematical methods capable of synchronously revealing signal characteristics in both the time and frequency domains, which is of great significance for processing non-stationary signals. As a typical non-stationary signal, seismic signals have frequency components that change with time and contain abundant geological information.²⁷ The traditional Fourier transform can only provide the global frequency distribution of signals and cannot characterize the local frequency evolution characteristics in the time dimension; therefore, time-frequency analysis methods play an irreplaceable role in seismic data interpretation and reservoir prediction.

The core of linear time-frequency analysis methods lies in constructing a time-frequency localized window function and characterizing the energy distribution of signals on the time-frequency plane through convolution operations between the window function and the signal. Specifically, such methods extract local features of signals at different times and frequencies through convolution operations between signals and time-window kernel functions, thereby realizing the time-frequency spectral characterization of non-stationary signals.

To further improve the resolution and stability of time-frequency analysis, inversion spectral decomposition methods introduce inversion concepts and sparse constraint regularization into the time-frequency analysis framework. Qin *et al.*²⁸ utilized the advantage of the generalized ST in flexibly adjusting the time-frequency window to construct a spectral decomposition

inversion model based on sparse constraints, significantly enhancing the energy concentration and resolution of time-frequency spectra. The key to this method is to reformulate the traditional linear transform process as an underdetermined linear inverse problem and obtain the optimal solution with clear physical significance by introducing the sparsity of signals in the time-frequency domain as a prior constraint.

In this study, the WT with adjustable time-frequency window characteristics is introduced to establish an inversion spectral decomposition model based on the WT. WT-ISD not only inherits the advantages of the sparse inversion framework in improving time-frequency resolution but also provides clearer physical significance and more flexible adjustment mechanisms for window function parameters. It can better adapt to the time-varying behavior of different frequency-band components in seismic signals by adjusting its time-frequency focusing characteristics, thereby providing a new technical approach for fine interpretation tasks such as fracture detection and thin-layer identification. The WT of a continuous-time signal $x(t)$ is defined as follows:

$$X(\tau, f) = \int_{-\infty}^{\infty} x(t)w(t-\tau; f)e^{-i2\pi ft} dt \quad (1)$$

where $X(\tau, f)$ is the time-frequency spectrum, τ is the time-shift parameter, and f is the frequency. The $w(t; f)$ employs an adjustable Gaussian window:

$$w(t; f) = \frac{\lambda f}{\sqrt{2\pi}} e^{-\frac{t^2 \lambda^2 f^2}{2}} \quad (2)$$

where λ is the scale factor, which is the core parameter balancing time-frequency resolution. An increase in λ narrows the time window, improving time resolution but reducing frequency resolution; conversely, a decrease in λ improves frequency resolution. The window function of the WT achieves continuous adjustment of time-frequency localization characteristics through a single parameter λ , and compared with the traditional ST, it has greater flexibility and adaptability.

The inverse WT ensures that signals can be completely reconstructed from their time-frequency spectra, and its expression reveals that signals can be represented as a linear combination of time-frequency atoms:

$$x(t) = \iint X(\tau, f)w(t-\tau, f)e^{i2\pi ft} df d\tau \quad (3)$$

The above inverse transform can also be explicitly expressed in the form of a convolution:

$$x(t) = \int [X(\tau, f) \otimes w(t, f)] e^{i2\pi ft} dt \quad (4)$$

where \otimes denotes the convolution operation. This expression provides a direct theoretical basis for constructing discrete inversion models. For numerical calculation, the continuous inverse transform formula is discretized. Let the discrete seismic signal be the vector $x = [x_{t_1} \ x_{t_2} \ \dots \ x_{t_N}]^T$, and the target frequency set be $\{f_1 \ f_2 \ \dots \ f_M\}$; the following discrete inversion model can be constructed:

$$\begin{bmatrix} x_{t_1} \\ x_{t_2} \\ \vdots \\ x_{t_N} \end{bmatrix} = \begin{bmatrix} G_{f_1} & G_{f_2} & \dots & G_{f_M} \end{bmatrix} \begin{bmatrix} m_{t_1, f_1} e^{i2\pi f_1 t_1} \\ \vdots \\ m_{t_N, f_1} e^{i2\pi f_1 t_N} \\ \vdots \\ m_{t_1, f_M} e^{i2\pi f_M t_1} \\ \vdots \\ m_{t_N, f_M} e^{i2\pi f_M t_N} \end{bmatrix} \quad (5)$$

where G_{f_i} is the convolution matrix composed of the Gaussian window function $w(t; f_i)$ corresponding to frequency f_i , and m is the vectorized form of the time-frequency coefficient matrix to be solved. **Equation 5** can be simplified as:

$$x = Gm \quad (6)$$

In seismic data analysis, x represents seismic records, G is the overcomplete dictionary matrix composed of WT window functions, and m is the high-resolution time-frequency spectrum to be solved. Since the reflection coefficient sequence usually satisfies the sparse distribution assumption, its time-frequency spectrum should also be sparse in the time-frequency domain, which provides a physical basis for introducing sparse constraints. Based on the prior sparsity of seismic signals in the time-frequency domain, the L1-norm sparse constraint is introduced to construct the following optimization problem:

$$\hat{m} = \arg \min_m \{ \|Gm - x\|_2^2 + \beta \|m\|_1 \} \quad (7)$$

where β is the regularization factor used to balance the weight between the data fitting term $\|Gm - x\|_2^2$ and the sparse constraint term $\|m\|_1$. An appropriate value of β can be determined through the L-curve method. This optimization problem is efficiently solved using the spectral projected gradient L1 minimization algorithm (SPGL1) to obtain the high-resolution time-frequency spectrum \hat{m} .

Based on the solved high-resolution time-frequency spectrum \hat{m} , high-fidelity frequency-divided processing can be realized under the inversion framework. For the target center frequency f_c , a Gaussian weight function $W(f; f_c, \sigma)$ is designed to weight the time-frequency spectrum:

$$m_{f_c} = \hat{m} \circ W(f; f_c, \sigma) \quad (8)$$

where \circ denotes the element-wise multiplication (Hadamard product) along the frequency dimension, and σ is the parameter controlling the frequency-divided bandwidth. The weighted time-frequency coefficient m_{f_c} is reconstructed through the inverse WT model to obtain the frequency-divided seismic data x_{f_c} corresponding to the frequency band:

$$x_{f_c} = Gm_{f_c} \quad (9)$$

This inversion and weighted reconstruction process is repeated for each trace in the 3D seismic data volume, and finally, a series of high-resolution frequency-divided data volumes reflecting the reflection characteristics of different frequency bands are obtained.

2.2. Spectral analysis performance

To systematically evaluate the performance of WT-ISD, a comparative analysis between WT-ISD and other time-frequency analysis methods was conducted. These methods include STFT, ST, and the WT. The comparison used both synthetic signals and actual seismic signals.

Firstly, comparative verification was performed based on synthetic signals. The synthetic signal was composed of three Ricker wavelets with dominant frequencies of 20 Hz, 35 Hz, and 50 Hz. Their time positions were set at 0.25 s, 0.55 s, and 0.85 s, respectively. The comparative results, as shown in [Figure 2](#), clearly illustrate the characteristics of each method. Limited by the fixed time window, STFT has acceptable resolution for the 20 Hz low-frequency wavelet. However, it exhibits significant energy diffusion and side lobe interference during time-frequency decomposition of the 35 Hz and 50 Hz wavelets, resulting in poor time-frequency focusing. ST can reflect the energy distribution of each frequency component but has insufficient time resolution in the low-frequency region, leading to blurred energy clusters.

In contrast, the WT introduces the instantaneous frequency parameter and a dynamic scale adjustment mechanism. It provides higher time resolution in the 20 Hz low-frequency band and enhances frequency resolution in the 50 Hz high-frequency band, thereby achieving overall optimization of time-frequency resolution. However, for strongly non-stationary signals with rapidly changing instantaneous frequencies (e.g., seismic data), the WT still suffers from energy diffusion due to its fixed parameterized window function. To address this limitation, WT-ISD realizes adaptive resolution optimization through sparse constraints. The results show that WT-ISD can significantly improve the focusing of time-frequency energy.

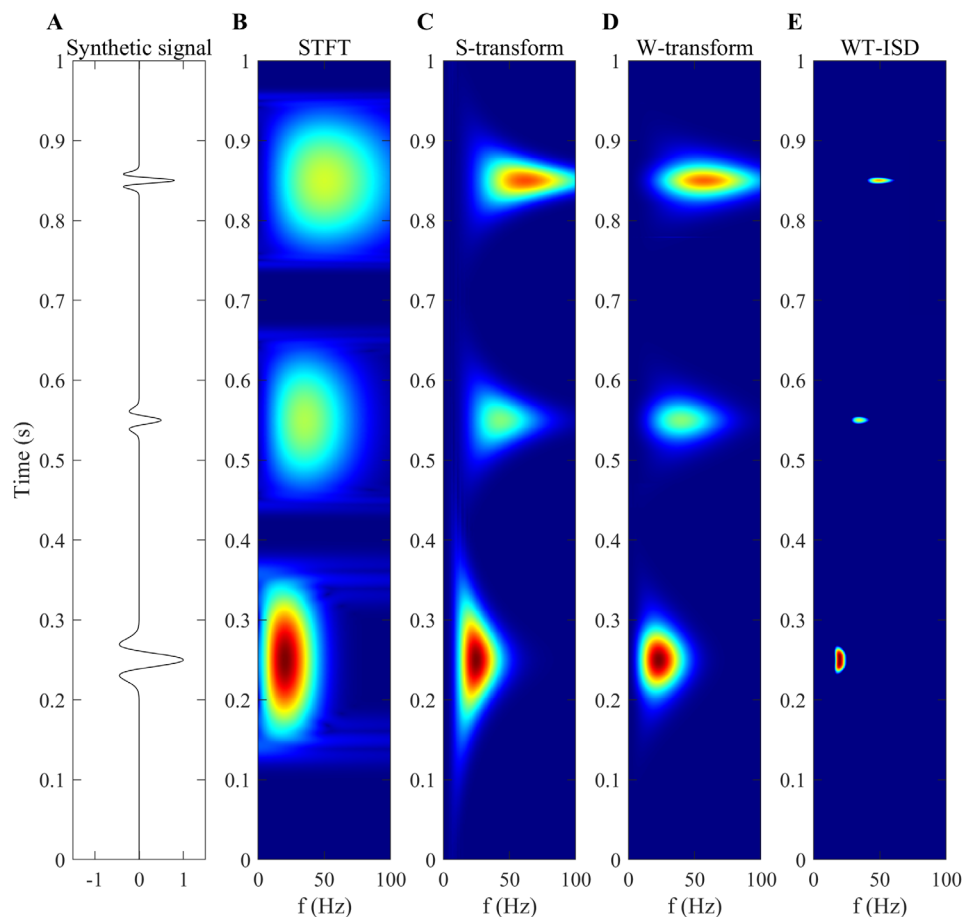


Figure 2. Spectrum of synthetic signal with different time–frequency analysis methods. (A) Synthetic signal. (B) STFT. (C) S-transform. (D) W-transform. (E) WT-ISD.

Abbreviations: STFT: Short-time Fourier transform; WT-ISD: W-transform inversion spectral decomposition.

To further verify the applicability of the method to actual seismic signals, a single-trace of actual seismic data from the study area was selected for testing. Figure 3 shows that WT-ISD also exhibits excellent performance when processing non-stationary and non-ideal actual seismic waveforms. The obtained time–frequency spectrum not only has the highest energy concentration, which enables finer characterization of the frequency evolution of effective signals over time, but also demonstrates stronger robustness against random noise, facilitating the identification and extraction of weak signals. The STFT and ST spectra show noticeable energy blurring, and although the WT effect is improved, its time–frequency localization details remain inferior to those of WT-ISD. Overall, WT-ISD outperforms other time–frequency analysis methods in both time–frequency resolution and noise suppression capability, providing a solid foundation for subsequent high-precision spectral decomposition and

effective extraction of frequency response characteristics of fractures of different scales.

3. Application examples

3.1. Regional geological overview

The Bongor Basin extends overall in a Northeast (NE)–Southeast (SE) direction, exhibiting a typical spindle-shaped geometry. It reaches a maximum width of 80 km at its central part and gradually tapers toward both ends, with a total area of approximately 1.8×10^4 km². The Raphia S block, the focus area of this study, is located in the northern slope belt of the basin, where the strata show a prominent wedge-shaped thinning trend toward the north. The northern slope belt hosts a multi-stage, genetically complex fault system, which can be divided into two categories based on their timing of formation: basement interior faults and basin-bounding faults. Basement interior faults

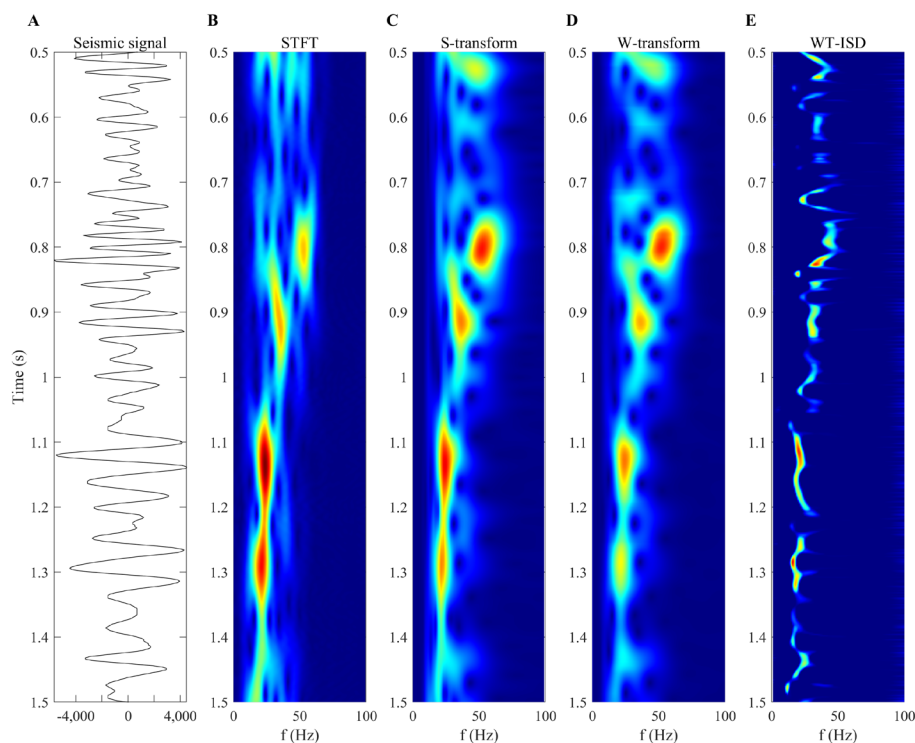


Figure 3. Spectrum of single channel seismic signal with different time–frequency analysis methods. (A) Seismic signal. (B) STFT. (C) S-transform. (D) W-transform. (E) WT-ISD.

Abbreviations: STFT: Short-time Fourier transform; WT-ISD: W-transform inversion spectral decomposition.

formed during the pre-rift stage of basin evolution and primarily control the internal structural differentiation of buried hills. Basin-bounding faults developed during the syn-rift and post-rift stages and dominate the structural evolution of the sags.

The basin is subdivided from south to north into four first-order tectonic units: the Southern Depression, Southern Uplift, Central Depression, and Northern Slope Belt (Figure 4). The Raphia buried hill belt, characterized by distinct structural features, is situated within the

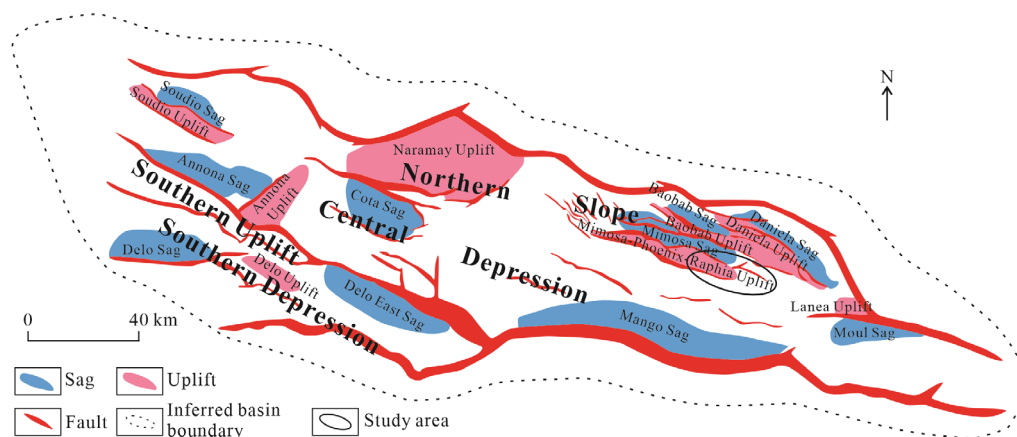


Figure 4. Tectonic units of bongor basin. Redrawn based on the data from yu *et al.*²⁹

Northern Slope Belt.

3.2. Spectral decomposition

Spectral decomposition techniques map seismic signals from the time domain to the frequency domain. By analyzing the evolutionary characteristics of amplitude and phase with frequency, they can effectively identify key geological information—including reservoir distribution, physical properties, and hydrocarbon potential.³⁰ This technique suppresses the mutual interference among different frequency components in the time domain, thereby delivering geological interpretations with higher resolution than conventional methods.

In this study, the WT-ISD method was employed for the time–frequency decomposition of seismic data. Its primary objective was to extract single-frequency data volumes corresponding to distinct frequency components, and the procedure consisted of a systematic sparse inversion and signal reconstruction workflow.

The method starts with trace-by-trace preprocessing of raw seismic data. This step includes obtaining analytic signals via the Hilbert transform and constructing an overcomplete dictionary matrix composed of frequency-dependent Gaussian window functions according to the target frequency band. The core innovation lies in reformulating the conventional WT as a basis pursuit denoising inverse problem. An L1-norm was introduced as a sparse constraint, and the optimal high-resolution time–frequency coefficient matrix was solved using SPGL1. Subsequently, within the inversion framework, a Gaussian frequency-weighting function centered at the target dominant frequency was designed. This function performs spectral focusing weighting on the time–frequency coefficients. The time-domain signals of the target frequency band were then accurately reconstructed using the adjoint of the dictionary matrix. Finally, the inversion and weighted reconstruction processes were implemented independently for each trace in the 3D seismic volume. A

Algorithm 1. W-transform inversion spectral decomposition

Inputs: 3D post-stack seismic data volume $X \in \mathbb{R}^{N_t \times N_f \times N_l}$, time sampling interval Δt , target frequency range $[f_{\min}, f_{\max}]$ with sampling Δf , scale factor λ , sparsity constraint parameter σ
Outputs: Frequency-divided seismic data volumes $\{X_{f_c}\}$ for each center frequency f_c
1: //Step 1: Construct overcomplete W-transform dictionary
2: Initialize frequency set $\mathcal{F} \leftarrow \{f_{\min}, f_{\min} + \Delta f, \dots, f_{\max}\}$
3: for each frequency $f_j \in \mathcal{F}$ do
4: Generate frequency-dependent Gaussian window: $w_j(t) = \frac{\lambda f_j}{\sqrt{2\pi}} \exp\left(-\frac{t^2 \lambda^2 f_j^2}{2}\right)$
5: Precompute window FFT: $\mathbf{W}_j, \mathbf{W}_j^{\text{flip}} \leftarrow \text{FFT}(w_j), \text{FFT}(\text{flip}(w_j))$
6: end for
7: Construct phase modulation matrix \mathbf{E} with $\mathbf{E}_{t,j} = e^{-i2\pi f_j t}$
8: //Step 2: Trace-wise sparse inversion (parallelizable)
9: for each seismic trace $\mathbf{x} \in \mathbf{X}(\text{dimension } N_t \times 1)$ do
10: Compute analytic signal: $\mathbf{x}_a \leftarrow \text{Hibert}(\mathbf{x})$
11: Define linear operator $\mathcal{A}(\mathbf{m}) = \mathbf{G}\mathbf{m}$, where \mathbf{G} encodes convolution with \mathbf{W}_j and modulation with \mathbf{E}
12: Solve basis pursuit denoising problem:
13: $\hat{\mathbf{m}} = \arg \min_{\mathbf{m}} \|\mathbf{m}\|_1$ s.t. $\|\mathcal{A}(\mathbf{m}) - \mathbf{x}_a\|_2 \leq \sigma$
14: Obtain time-frequency coefficient matrix $\mathbf{M} \in \mathbb{R}^{N_t \times |\mathcal{F}|}$ via SPGL1 algorithm
15: Store \mathbf{M} to \mathbf{M}_{all}
16: end for
17: //Step 3: Frequency band extraction and reconstruction
18: for each target center frequency f_c do
19: Construct Gaussian weight vector: $\mathbf{v}_c(f) = \exp\left(-\frac{f^2}{2f_c^2}\right)$
20: for each time–frequency matrix \mathbf{M} do
21: Apply frequency weighting: $\mathbf{M}_c \leftarrow \mathbf{M} \odot \mathbf{v}_c$
22: Reconstruct single-frequency signal: $\mathbf{x}_{f_c} \leftarrow \text{Real}(\mathcal{A}^*(\mathbf{M}_c))$
23: end for
24: Combine all \mathbf{x}_{f_c} to form frequency-divided volume \mathbf{X}_{f_c}
25: end for
26: return $\{\mathbf{X}_{f_c}\}$
Key parameters:
 λ : Scale factor balancing time–frequency resolution (typically 1.0–4.0)
 σ : Inversion tolerance controlling sparsity level
 β : Gaussian bandwidth controlling frequency division sharpness

Abbreviations: 3D: Three-dimensional; FFT: Fast Fourier transform; SPGL1: Spectral projected gradient for L1 minimization algorithm.

series of high-resolution frequency-divided data volumes with concentrated energy and clear boundaries are efficiently generated via parallel computing.

Notably, the WT-ISD method incorporates an L1-norm sparse constraint. It transforms conventional linear time-frequency analysis into a model-driven nonlinear inversion problem, whose solution relies on the iterative optimization of the SPGL1 algorithm. As a result, its computational load is significantly higher than that of traditional closed-form time-frequency transforms.

The major computational overhead stems from two sources. The first is the construction of the frequency dictionary and convolution kernels, along with the subsequent convolution operations. The second is the multiple iterations of sparse inversion and repeated applications of linear operators. The computational complexity increases approximately linearly with the frequency sampling density and the length of the time window, and is further modulated by the number of iterations and convergence tolerance. To mitigate this computational burden, a single inversion, multi-frequency reconstruction strategy was adopted in this study. Only one SPGL1-based sparse inversion was performed per trace to obtain the time-frequency coefficients. All subsequent dominant-frequency data volumes are generated from these coefficients through efficient convolution and linear combinations of frequency-band weights. This design avoids repeated L1-norm iterations for each individual frequency band.

Meanwhile, the fast Fourier transform of frequency-dependent Gaussian windows and the dominant-frequency weight matrix were precomputed and reused at the beginning of the experiment. This measure substantially reduces the overhead of inner-loop operations. Trace-by-trace processing was parallelized across a multi-core platform. Additionally, the maximum number of iterations and convergence tolerance were constrained to control computational costs. This implementation achieves acceptable overall computational efficiency while preserving the advantage of high time-frequency resolution, meeting the demands of large-scale seismic volume processing.

In essence, WT-ISD upgrades linear time-frequency analysis to a model-driven sparse inversion framework. It effectively overcomes the inherent limitations on time-frequency resolution imposed by the Heisenberg uncertainty principle. Accordingly, it provides a reliable foundation of time-frequency features for spectrum-based fine reservoir characterization.

In practical implementation, WT-ISD is directly

applied to the full-area 3D seismic data. Spectral analysis is first conducted to determine the dominant frequency band of the dataset. Using this high-precision time-frequency method, 12 single-frequency seismic data volumes with distinctly dominant frequencies are extracted within the effective frequency band.

To systematically evaluate the response relationship between frequency and fracture scale, 12 characteristic frequency-divided data volumes covering 5–60 Hz were selected. By comparing the spatial responses of different frequency volumes to structural discontinuities and stratigraphic attributes, the indicative relationships between frequency and fracture development scale were established. The findings revealed that low-frequency volumes show strong responses to the outlines of large-scale faults, medium-frequency volumes achieve optimal performance in identifying medium-scale fracture zones, and high-frequency volumes exhibit high sensitivity to microfractures and subtle geological features.

Figure 5 presents the original seismic profile and the spectral analysis results of the raw seismic data. Additionally, Figure 6 displays the seismic profiles of the 12 frequency-divided data volumes with different dominant frequencies after spectral decomposition. The results demonstrate that each single-frequency volume highlights structural and stratigraphic information of different hierarchical levels. Low-frequency volumes clearly delineate the planar distribution of large-scale faults. Medium-frequency volumes reveal more abundant internal structural details while retaining the outlines of major faults. High-frequency volumes further enhance the response signals of minor faults and small-scale fractures. These frequency-divided data volumes effectively separate the seismic response characteristics of geological bodies at different scales. They provide high-quality input data for subsequent discontinuity detection and multi-scale fracture identification using frequency-divided ant-tracking method.

3.3. Data preprocessing

Structure-oriented filtering technology, a key method in seismic data processing, can effectively utilize the dip angle and azimuth angle information of geological targets, significantly improving the accuracy of attribute prediction and the detection efficiency of target bodies. While enhancing the signal-to-noise ratio of the seismic data volume and preserving the basic characteristics of the original seismic signals, this technology can specifically strengthen the discontinuity of seismic events, generate clearer imaging of faults and fractures, and provide robust support for the accurate identification of micro-faults.³¹

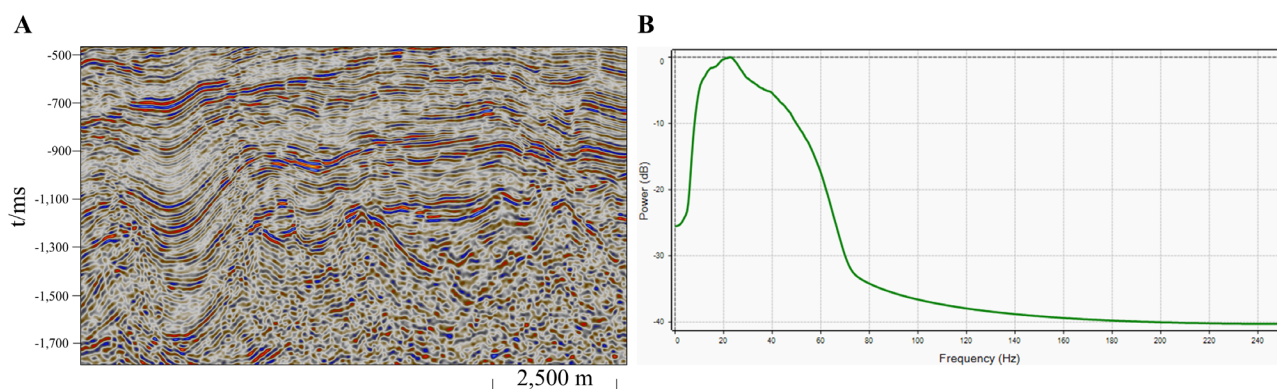


Figure 5. Original seismic profile and spectral analysis results of the raw seismic data in the Raphia S Block, Bongor Basin. (A) Post-stack seismic profile (scale bar = 2,500 m) and (B) amplitude spectrum analysis result of the raw seismic data, showing the power distribution variation with frequency.

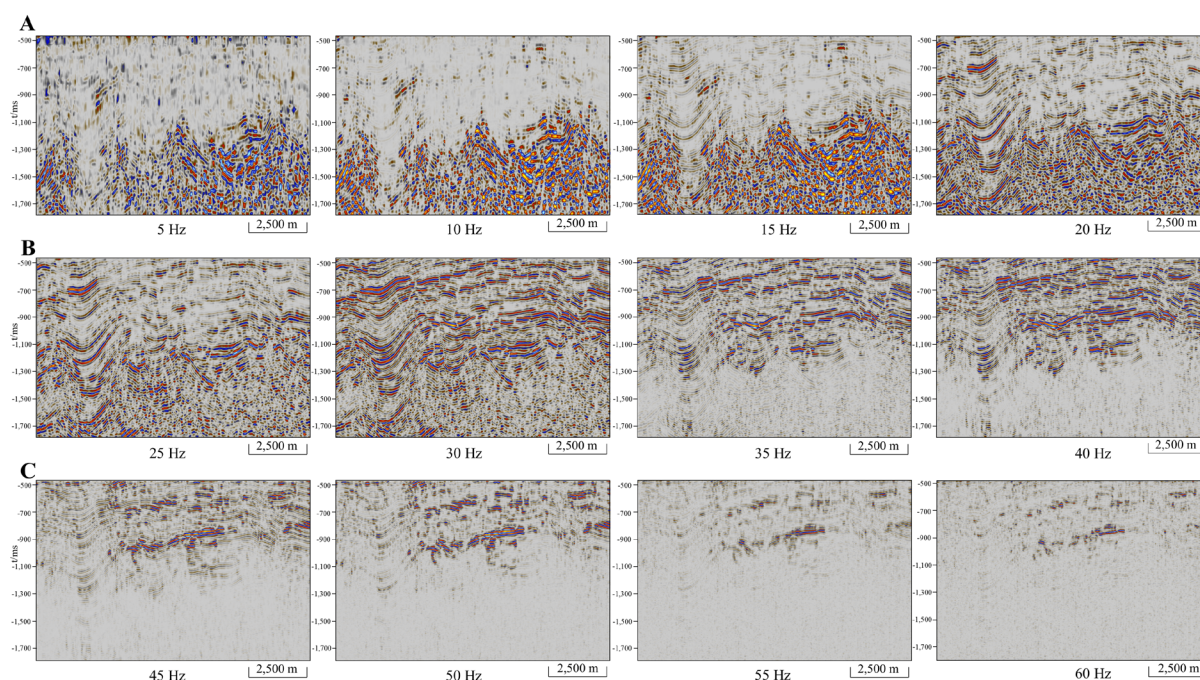


Figure 6. Single-frequency seismic profiles (scale bar = 2,500 m): (A) Low-, (B) medium-, and (C) high-frequency bands

Figure 7 shows the processing effects of frequency-divided ant volumes in different frequency bands after structure-oriented filtering. By comparing the results before and after filtering, it can be observed that the random noise in the original seismic data has been effectively suppressed, the continuity of seismic events is significantly improved, and the fault boundary characteristics within the dashed box are more prominent, thereby laying a solid foundation for the subsequent detailed characterization of fracture systems.

3.4. Discontinuity detection

After structure-oriented filtering, the resolution and clarity

of faults have been improved to a certain extent, but some faults still suffer from issues such as blurred boundaries and insufficient spatial continuity. To address this limitation, discontinuity detection technology was further adopted to enhance the spatial continuity of fractures and highlight fault boundary characteristics.

Currently, there are several commonly used discontinuity detection methods, whose applicability and performance vary significantly depending on the geological conditions of different study areas. Among them, the variance volume attribute, as a classic post-stack seismic attribute, offers advantages of wide applicability and stable identification performance, making it a commonly used

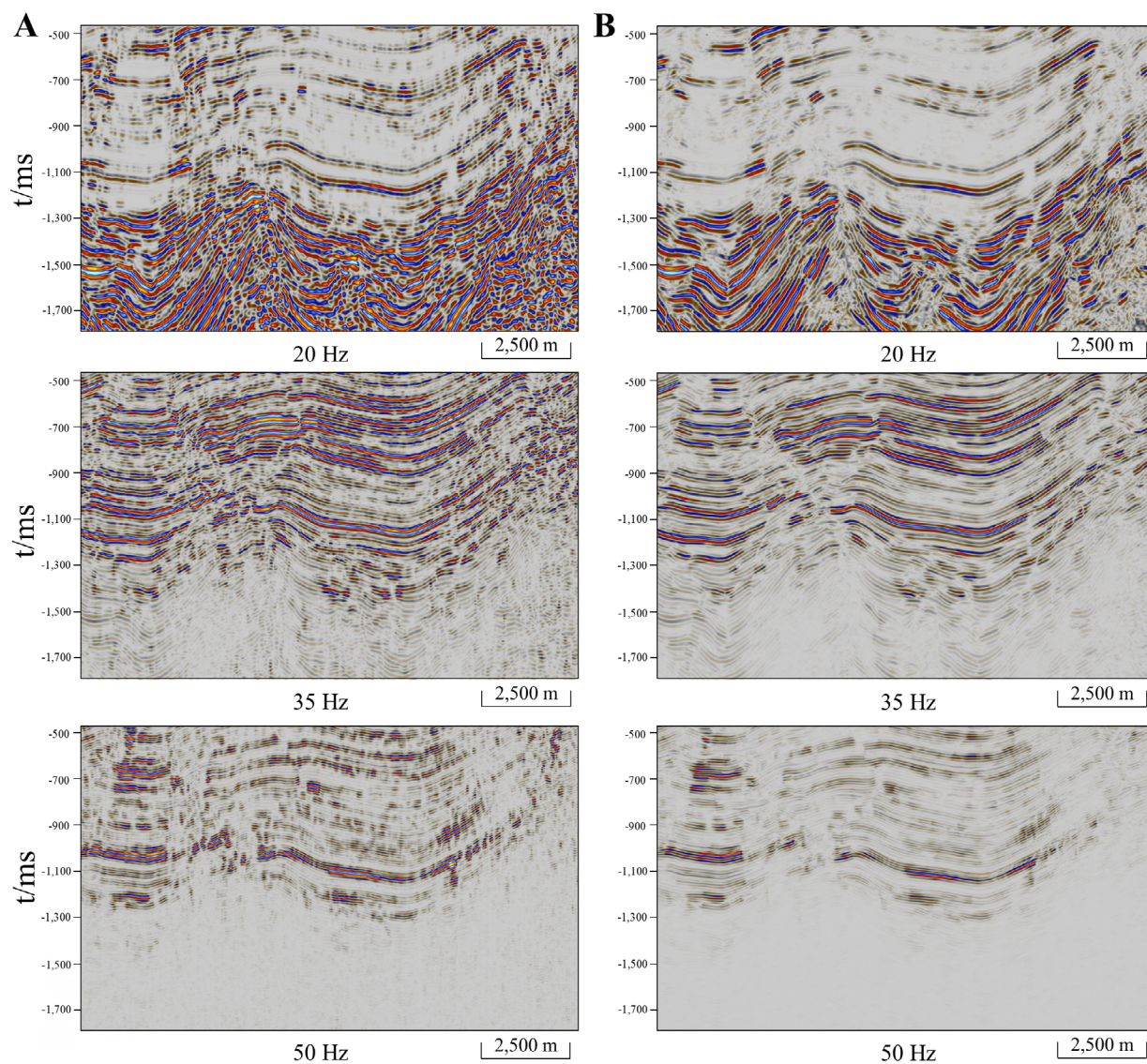


Figure 7. Structure-oriented filtering results (scale bar = 2,500 m): (A) Frequency-divided seismic profile before filtering and (B) frequency-divided seismic profile after structure-oriented filtering

and effective method for fault boundary identification.³²

The variance attribute constructs a variance volume by calculating the amplitude variance between each seismic trace in the trace gather and the average seismic trace. Its core lies in characterizing the differences in reflection characteristics between adjacent seismic traces (mainly reflected in amplitude variations), thereby exploring abnormal seismic reflection information caused by anomalous geological bodies or faults, and ultimately achieving the effective identification of faults and fractures.

Figure 8 presents the horizon slice results of 12 variance volumes with distinct dominant frequencies. The comparative analysis demonstrates that within the low-frequency band (5–20 Hz), the 20 Hz variance volume

provides the clearest delineation of large-scale fractures. Additionally, within the medium-frequency band (25–40 Hz), the 35 Hz variance volume achieves optimal performance in identifying medium-scale fractures. In the high-frequency band (45–60 Hz), the 50 Hz variance volume shows the best effect in characterizing densely distributed small-scale fractures. Accordingly, these three single-frequency variance data volumes are ultimately selected as the input data for subsequent high-quality frequency-divided ant-tracking.

3.5. Attitude-constrained frequency-divided ant-tracking

The identification performance of the ant-tracking

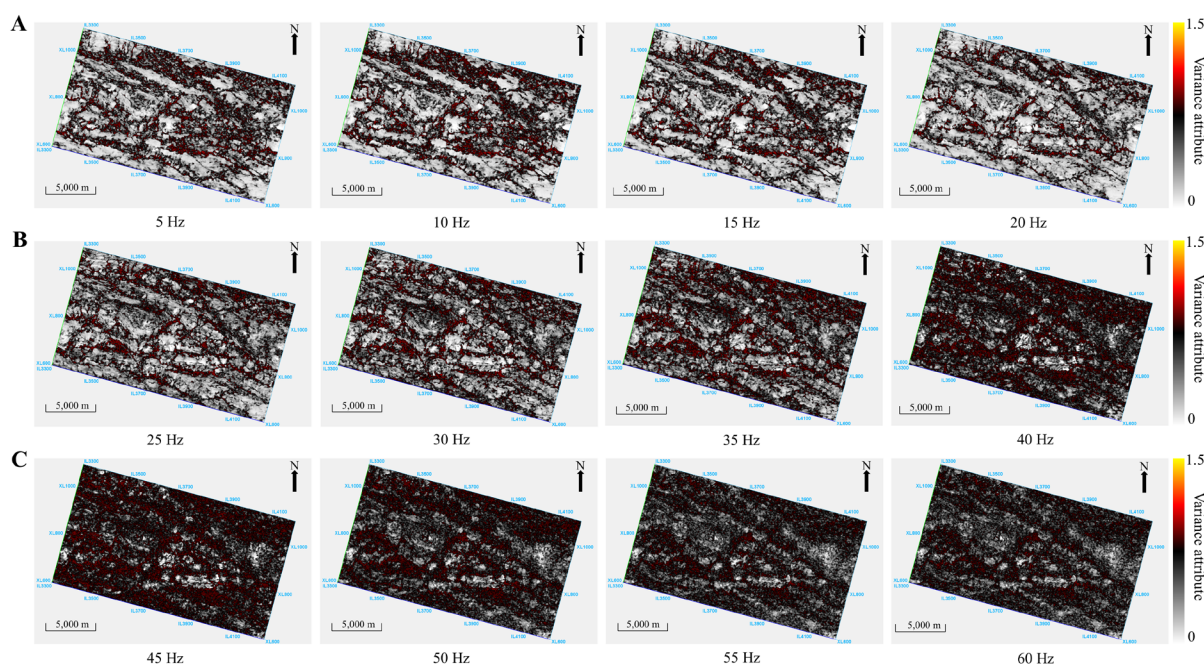


Figure 8. Horizon slices of discontinuity detection for frequency-divided seismic data volumes (scale bar = 5,000 m): (A) Low-, (B) medium-, and (C) high-frequency bands.

algorithm is mainly jointly constrained by algorithm parameter settings and regional structural background characteristics. In this study, the active ant-tracking algorithm was adopted. This algorithm focuses on refined search in local areas, features a short step length and low deviation tolerance, and is more suitable for the precise characterization of fracture systems under complex structural backgrounds. After optimizing and selecting the ant-tracking parameter combination, it is still necessary to introduce an attitude constraint mechanism. Without the constraint of regional structural characteristics, ant-tracking will perform omnidirectional, undifferentiated fracture search, but fracture development in the actual study area has significant directionality and is not randomly distributed in all directions, making the tracking results prone to false fractures. The attitude-constrained ant-tracking method is thus a key means to eliminate false fracture information and improve identification reliability.

The specific implementation process is as follows: based on the generated single-frequency seismic attribute data volumes, combined with previous research findings, key attitude parameters such as the strike, dip direction, and dip angle of major faults in the area were statistically analyzed to clarify the spatial distribution patterns of fracture development, and targeted filtering criteria were subsequently formulated. Meanwhile, considering that horizon reflection traces usually exhibit low-dip angle responses, low-dip angle anomalies need to be filtered

out. During the actual ant-tracking process, precise control of the search direction was achieved through the stereographic projection diagram in Petrel E&P software platform (2018, Schlumberger Limited, France; Figure 9). The dip angle and azimuth range of fractures to be filtered out are set as the gray area, and fractures within this range will not be included in the tracking results. In contrast, fractures corresponding to the white area are the target objects of ant-tracking and will be recorded.

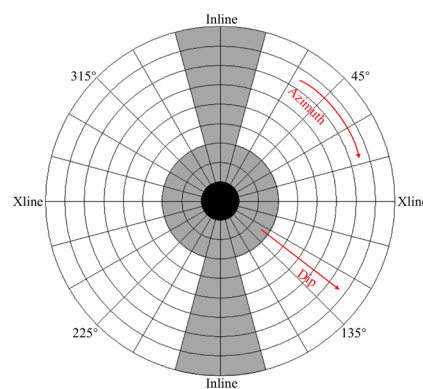


Figure 9. Stereonet map generated using attitude-constrained ant-tracking in Petrel E&P software platform

Previous studies have shown that the Raphia buried hill belt extends in a Northwest (NW)–SE direction, with a length of approximately 20 km, a width of about 5 km,

and a structural area of around 100 km². Controlled by NW-trending major faults, the buried hill belt generally strikes NW–SE, and the mountain tops from South to North exhibit an en-echelon distribution pattern. A NW-trending mountain ridge develops along the line of Raphia SW-2–Raphia S-3–Raphia S-11–Raphia S-9 within the buried hill belt, and the burial depth gradually decreases from NW to SE, with a maximum burial depth of about –500 m, a minimum burial depth of approximately –1,900 m, and a maximum vertical drop of up to 1,400 m, forming multiple fault-block mountains with significant height differences.

Three sets of faults are mainly developed in the Raphia S buried hill belt (Figure 10). The first set is approximately NW–NW-west (NNW) trending faults, which serve as major faults in the area and control the formation and spatial distribution of the buried hill belt. The second set is approximately Eastwest (EW)-trending faults, which function to divide the buried hill belt into blocks and significantly control the development of buried

hill fractures. The third set is near NE-trending faults, which cut the NW-trending major faults, complicate the internal structure of the buried hill, and play a key role in promoting the formation and development of buried hill fractures. Detailed characteristics of the main faults in the Raphia buried hill belt are shown in Table 1.

Based on the actual geological conditions of the Raphia S block, the dip angle range of faults participating in the ant-tracking calculation was finally set to 60–90° (as nearly vertical strike-slip faults develop in the area, 90° was selected as the maximum dip angle threshold). In terms of azimuth, NW–NNW, approximately EW, and NE-trending fractures are retained for calculation.

Under attitude constraints, ant-tracking was performed on the single-frequency variance data volumes of 20 Hz, 35 Hz, and 50 Hz, respectively, with the results shown in Figure 11. The 20 Hz low-frequency ant volume (Figure 11A) clearly depicts the planar distribution of large-scale NW–NNW trending faults that control the buried hill framework. The 35 Hz medium-frequency ant

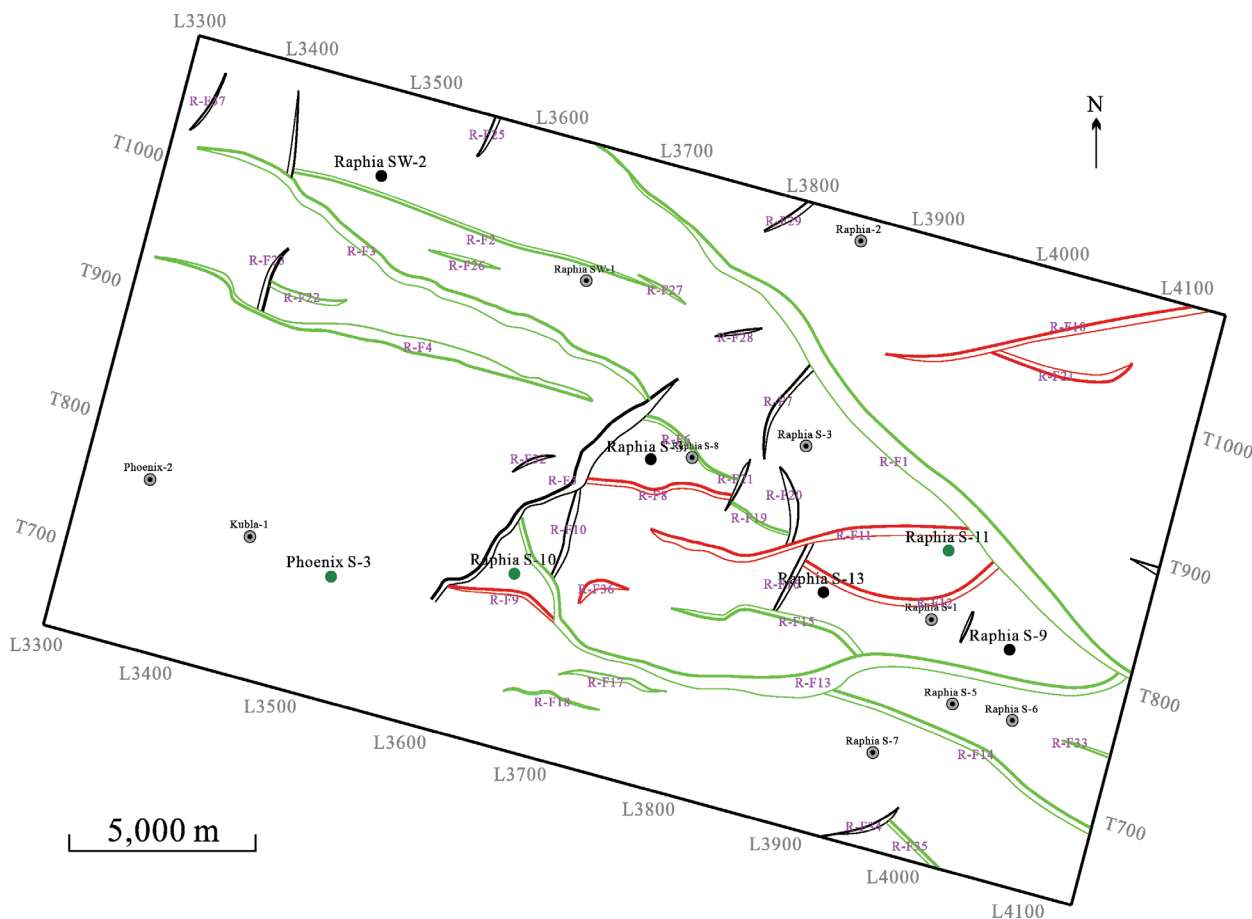


Figure 10. Fault distribution map of the Raphia S buried hill belt (scale bar = 5,000 m). The first fault set is highlighted in green, the second set in red, and the third set in black.

Table 1. Main fault elements of Raphia S block buried hill belt

| Fault name | Fault type | Strike | Azimuth | Dip angle (°) |
|------------|--------------|--------|---------|---------------|
| R-F1 | Normal fault | NW | NE | 65–80 |
| R-F2 | Normal fault | NWW | SSW | 60–80 |
| R-F3 | Normal fault | NW | NE | 70–80 |
| R-F4 | Normal fault | NWW | SSW | 70–85 |
| R-F5 | Normal fault | NE | NW | 70–80 |
| R-F6 | Normal fault | NW | NE | 65–80 |
| R-F7 | Normal fault | NE | NW | 60–80 |
| R-F8 | Normal fault | EW | N | 70–80 |
| R-F9 | Normal fault | EW | S | 65–80 |
| R-F10 | Normal fault | EW | NWW | 65–85 |
| R-F11 | Normal fault | EW | N | 55–70 |
| R-F12 | Normal fault | EW | N | 60–75 |
| R-F13 | Normal fault | EW | N | 65–80 |
| R-F14 | Normal fault | NW | NE | 65–70 |
| R-F15 | Normal fault | NWW | SSW | 60–80 |
| R-F16 | Normal fault | NE | NW | 65–80 |

Abbreviations: EW: Eastwest; N: North; NE: Northeast; NW: Northwest; NWW: Northwest-west; S: South; SSW: South-southwest.

volume (Figure 11B) retains the outline of large faults and reveals more abundant medium-scale fractures, especially enhancing the response to near-EW and NE trending fractures. The 50 Hz high-frequency ant volume (Figure 11C) further identifies a large number of densely distributed small-scale fractures with the richest detailed information. This frequency-divided processing strategy effectively achieves the separation and identification of multi-scale fracture systems from large-scale to small-scale fractures.

4. Application results

To systematically verify the high precision, high resolution, and refined characterization capability of the frequency-divided ant-tracking method based on WT-ISD in fracture prediction, three fracture prediction approaches were selected for application and comparative analysis. These approaches include conventional ant-tracking,

frequency-divided ant-tracking based on conventional ST, and frequency-divided ant-tracking based on WT-ISD. Comprehensive comparative verification was conducted from both seismic profile and planar dimensions.

Before the verification, RGB attribute fusion was first performed on three sets of single-frequency ant volume data. These data were obtained through frequency division processing via ST and WT-ISD, with each set corresponding to a distinct dominant frequency. RGB fusion is not a simple image superposition—its scientific validity depends on the assignment of reasonable weights. Correlation analysis was conducted between the fault polygons of the Raphia S block and the ant volumes at dominant frequencies of 20 Hz, 35 Hz, and 50 Hz. A higher correlation corresponds to a larger weight. The correlation analysis results indicate that the weight coefficients of the 20 Hz, 35 Hz, and 50 Hz ant volumes are 0.5, 0.35, and 0.15, respectively. Based on this weight scheme, attribute-weighted fusion was completed

for the three sets of single-frequency ant volumes with different dominant frequencies.

In the profile verification stage, three sets of results were superimposed on the original seismic profile for comparative display, including the conventional ant-tracking results (Figure 12A), the attribute-fused frequency-divided ant-tracking results based on conventional ST (Figure 12B), and the attribute-fused frequency-divided ant-tracking results based on WT-ISD (Figure 12C). This display is designed to visually reveal the spatial distribution characteristics of the fault system. As illustrated in Figure 12, the consistency between fractures identified by conventional ant-tracking and seismic reflection features is significantly lower than that of the frequency-divided ant volume results integrated across multiple frequencies. Compared with the attribute-fused ant volumes derived from ST-based frequency division, the attribute-fused ant volumes obtained from WT-ISD-based frequency division exhibit superior performance. They can characterize fractures of all scales more clearly, identify a notably greater number of fractures, and present more complete continuity of fault structures in the profile space.

In the planar characteristic analysis stage, the WT-ISD-based frequency-divided ant-tracking results processed via RGB attribute fusion were visualized.

Finally, a comprehensive fracture prediction map of the study area was generated (Figure 13). This fused result effectively integrates the seismic response characteristics of fractures at different scales across all frequency bands. It also highlights the complementary contribution of multi-frequency information in fracture detection. Accordingly, a more comprehensive and refined characterization of the fracture network in the study area is achieved.

To further verify the superiority of the proposed WT-ISD-based frequency-divided ant-tracking method, a systematic comparison was conducted among three sets of results—the conventional ant-tracking results (Figure 14A), the ST-based frequency-divided ant-tracking results (Figure 14B), and the WT-ISD-based frequency-divided ant-tracking results (Figure 14C).

The analysis demonstrates that the prediction outcomes of the WT-ISD-based frequency-divided ant-tracking method are significantly superior to those of the other two methods across multiple evaluation indicators. In terms of the richness of fracture identification, frequency division processing effectively separates the frequency response characteristics of fractures at different scales. This enables the ant volumes to clearly characterize large-, medium-, and small-scale fracture systems. The number of identified fractures increases markedly, and the structural framework

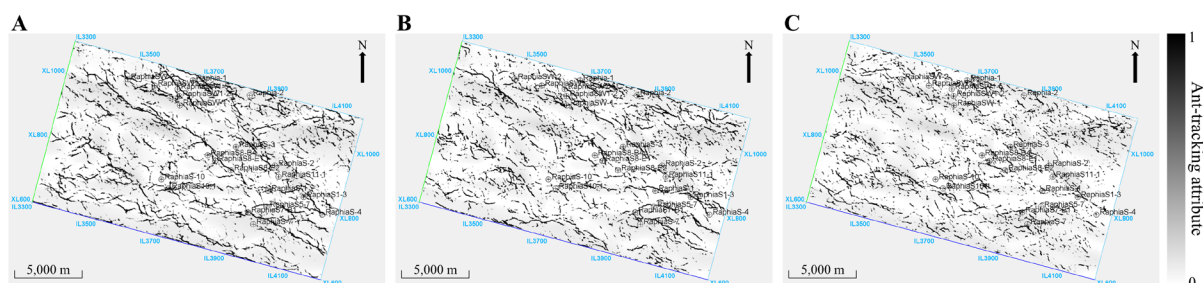


Figure 11. Horizon slices of attitude-constrained frequency-divided ant-tracking for the buried hill horizon (scale bar = 5,000 m): (A) 20 Hz ant volume, (B) 35 Hz ant volume, and (C) 50 Hz ant volume

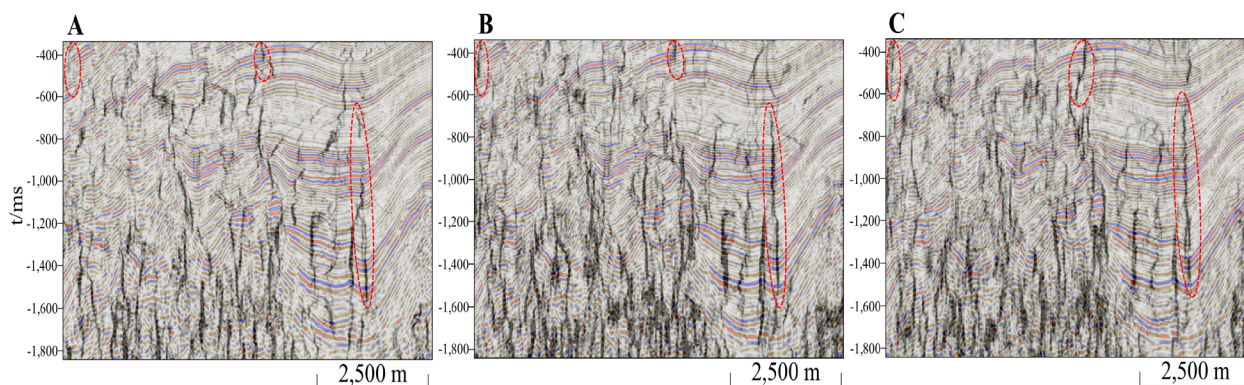


Figure 12. Comparative verification of ant-tracking results along the seismic profile (scale bar = 2,500 m). (A) Conventional ant-tracking. (B) Frequency-divided ant-tracking based on conventional S-transform. (C) Frequency-divided ant-tracking based on W-transform inversion spectral decomposition.

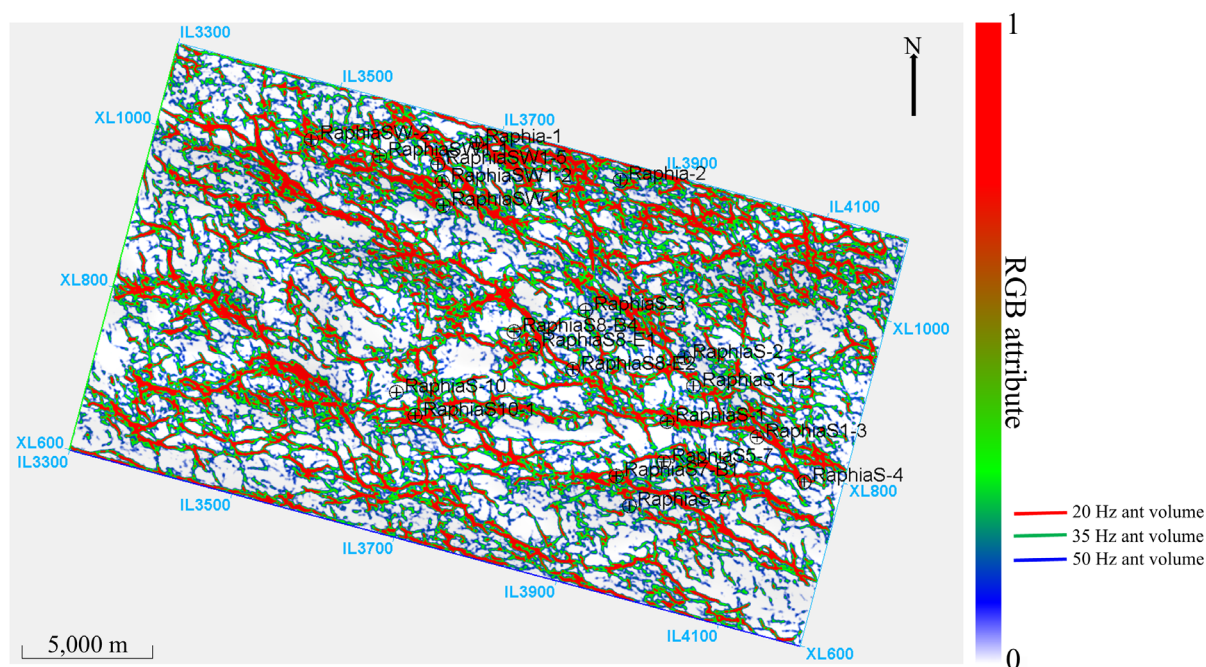


Figure 13. Red–green–blue (RGB) attribute fusion results of W-transform inversion spectral decomposition-based frequency-divided ant-tracking (scale bar = 5,000 m)

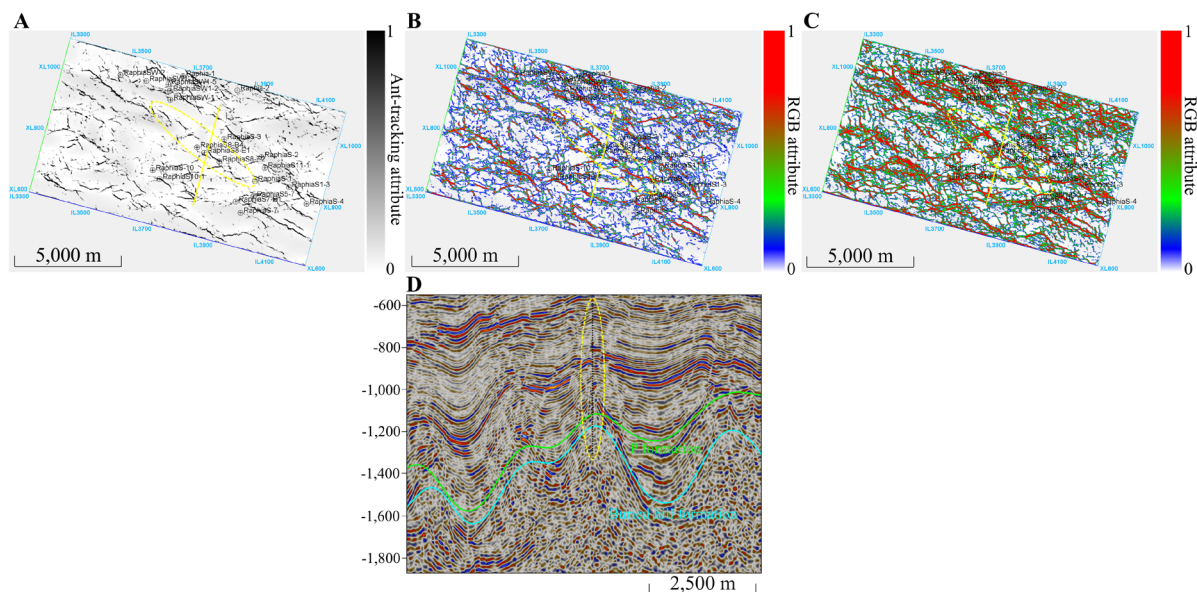


Figure 14. Comparison of three ant-tracking fracture prediction methods. (A) Conventional ant-tracking (scale bar = 5,000 m). (B) S-transform-based frequency-divided ant-tracking (scale bar = 5,000 m). (C) W-transform inversion spectral decomposition-based frequency-divided ant-tracking (scale bar = 5,000 m). (D) Seismic profile across the study area showing the P formation and buried hill formation, where the fracture system within the yellow dashed circle corresponds to the fracture system marked by the yellow dashed circle in the planar results of (A)–(C) (scale bar = 2,500 m).

of the fracture system becomes more complete.

In terms of the spatial continuity of faults, the fault distribution presented by the frequency-divided ant volumes exhibits higher coherence and integrity. The

continuous identification ability is significantly enhanced, especially when tracking major fault systems with a wide extension range. In terms of consistency with the structural strike, the frequency-divided results are highly consistent

with the fault distribution characteristics of the buried hill belt in the Raphia S block, indicating strong geological conformity. Notably, in the identification of NW–NWW-trending major faults, the frequency-divided ant volumes obtained based on WT-ISD have clear boundaries and regular morphologies. This represents a remarkable improvement over the problems of blurred fault boundaries and insufficient continuity in the other two methods. This improvement effectively enhances the interpretability and reliability of the fracture prediction results.

5. Conclusion

In this study, a frequency-divided ant-tracking method based on WT-ISD was systematically developed and validated, successfully overcoming the limitations of conventional ant-tracking, such as sensitivity to data quality and poor continuity of fault identification. Comprehensive tests on actual seismic data from the Raphia S Block in the Bongor Basin yielded the following key conclusions:

- (i) The WT-ISD achieves substantial advancements in algorithm design and functional performance for time–frequency analysis. Algorithmically, it innovatively integrates sparse inversion theory with the WT, constructing an overcomplete dictionary matrix and introducing L1-norm sparsity constraints. Solved via the SPGL1 algorithm, this framework transforms traditional linear time–frequency analysis into a model-driven nonlinear inversion process. Functionally, WT-ISD effectively breaks the inherent time–frequency resolution trade-off imposed by the Heisenberg uncertainty principle that constrains conventional linear methods. It delivers time–frequency spectra with superior energy concentration, higher resolution, and enhanced noise resistance, enabling precise characterization of time–frequency responses from multi-scale geological bodies (e.g., fractures, thin layers). Beyond fracture prediction, this advancement provides a robust tool for high-fidelity non-stationary signal decomposition, with broad implications for geophysical signal processing and related interdisciplinary fields.
- (ii) The frequency-divided fracture prediction workflow exhibits strong generalizability and excellent multi-scale fracture identification capability. Application results confirm that extracting single-frequency data volumes sensitive to 20 Hz (large-scale fractures), 35 Hz (medium-scale fractures), and 50 Hz (small-scale fractures) enables effective separation and refined characterization of multi-scale fracture systems. The final RGB-fused fracture model outperforms conventional methods in fracture richness, spatial continuity, and consistency with regional structures.

This workflow is not limited to the Bongor Basin; its data-driven design allows flexible adjustment of key parameters (e.g., frequency bands, attitude constraints, fusion weights) to adapt to different basin types (e.g., rift basins, foreland basins) and fracture systems (e.g., tectonic, diagenetic, hybrid), providing a practical solution for accurate multi-scale fracture characterization in complex reservoirs.

Acknowledgments

None.

Funding

This research was supported by the Open Fund Project (Tenth Batch) (Grant No. K2024-03) of the Key Laboratory of Oil and Gas Resources and Exploration Technology, Ministry of Education, Yangtze University, China.

Conflict of interest

The authors declare they have no competing interests.

Author contributions

Conceptualization: Ying Jia, Xilin Qin
Formal analysis: Xiuwei Wang, Xilin Qin
Funding acquisition: Ying Jia, Xiuwei Wang
Investigation: Ying Jia, Jun Wang
Methodology: Xilin Qin, Yinglong Li
Project administration: Ying Jia, Xiuwei Wang
Validation: Yinglong Li
Visualization: Xilin Qin, Yinglong Li
Writing–original draft: Ying Jia, Yinglong Li
Writing–review & editing: Ying Jia, Xilin Qin

Availability of data

Data are available from the corresponding author upon reasonable request.

References

1. Liu YW, Liu XW, Han L, Liu ZY. Development status of seismic fracture prediction technology. *World Pet Ind.* 2024;31(3):26–34. [In Chinese].
doi: 10.20114/j.issn.1006-0030.20240130001
2. Du X, Fan TE, Fan PJ, Ma TF, Zhang XW. Seismic prediction method of multi-scale fracture zone for buried-hill fractured reservoir. *Chin J Geophys.* 2024;67(8):3184–3195. [In Chinese].
doi: 10.6038/cjg2024R0451
3. Zhu BH. Improved Ant Tracking Crack Detection Algorithm and Its Application. *Offshore Oil.* 2019;39(3):27–32. [In Chinese].

- doi: 10.3969/j.issn.1008-2336.2019.03.027
4. Liang ZQ. Poststack seismic prediction techniques for fractures of different scales. *Geophys Prospect Pet.* 2019;58(5):766-772.
doi: 10.3969/j.issn.1000-1441.2019.05.016
 5. Portnoff M. Time-frequency representation of digital signals and systems based on short-time Fourier analysis. *IEEE Trans Acoust Speech Signal Process.* 1980;28(1):55-69.
doi: 10.1109/tassp.1980.1163359
 6. Uesugi F. Novel image processing method inspired by wavelet transform. *Micron.* 2023;168:103442.
doi: 10.1016/j.micron.2023.103442
 7. Stockwell RG, Mansinha L, Lowe RP. Localization of the complex spectrum: the S transform. *IEEE Trans Signal Process.* 1996;44(4):998-1001.
doi: 10.1109/78.492555
 8. Zhao ZC, Rao Y, Wang YH. Structure-adapted Multichannel Matching Pursuit for Seismic Trace Decomposition. *Pure Appl Geophys.* 2023;180(3):851-861.
doi: 10.1007/s00024-023-03234-w
 9. Daubechies I, Lu J, Wu HT. Synchrosqueezed wavelet transforms: An empirical mode decomposition-like tool. *Appl Comput Harmon Anal.* 2011;30(2):243-261.
doi: 10.1016/j.acha.2010.08.002
 10. Zhang GL, Duan J, Li Y, He CJ, Du H, Luo F. Adaptive Time-Resampled High-Resolution Synchrosqueezing Transform and Its Application in Seismic Data. *IEEE Trans Geosci Remote Sens.* 2020;58(9):6691-6698.
doi: 10.1109/TGRS.2020.2978509
 11. Partyka G, Gridley J, Lopez J. Interpretational applications of spectral decomposition in reservoir characterization. *Lead Edge.* 1999;18(3):353-360.
doi: 10.1190/1.1438295
 12. Zeng H, John A, G JK. Frequency-dependent Seismic Stratigraphy. In: *Proceedings of the SEG Technical Program Expanded Abstracts 2009*. 79th SEG Annual International Meeting; October 5–30, 2009; Houston, Texas, USA. Society of Exploration Geophysicists; 2009:1097-1101.
doi: 10.1190/1.3255040
 13. Wang YH. The W transform. *Geophysics.* 2021;86(1):31-39.
doi: 10.1190/geo2020-0316.1
 14. Li R, Zhu X, Zhou YZ, Chen H, Chen XP, Hu Y. Generalized W transform and its application in gas-bearing reservoir characterization. *IEEE Geosci Remote Sens Lett.* 2021;19:1-5.
doi: 10.1109/LGRS.2021.3108836
 15. Chen H, Peng L, Chen XP, Hu Y, Li R, Fang YX. A three-parameter W transform and its application to gas reservoir identification. *Geophysics.* 2022;87(5):V521-V532.
doi: 10.1190/geo2021-0803.1
 16. Luo CP, Zong ZY. The synchroextracting algorithm based on W transform and its application in channel characterization. *IEEE Geosci Remote Sens Lett.* 2023;20:1-5.
doi: 10.1109/LGRS.2023.3262637
 17. Chen XP, Hu Y, Chen H, Wen XT, Guo S. The Normalized W Transform for Seismic Interpretation. *Geophysics.* 2025;90(5):V421-V438.
doi: 10.1190/geo2024-0678.1
 18. Dorigo M, Maniezzo V, Colorni A. Ant system: optimization by a colony of cooperating agents. *IEEE Trans Syst Man Cybern B Cybern.* 1996;26(1):29-41.
doi: 10.1109/3477.484436
 19. Yuan YO, Simons FJ. Multiscale adjoint waveform-difference tomography using wavelets. *Geophysics.* 2014;79(3):WA79-WA95.
doi: 10.1190/geo2013-0383.1
 20. Wen H, Wang Z, Ding LM, et al. Fracture detection method of messy body attribute based on multichannel synchro squeezing generalized S-transform. *Prog Geophys.* 2025;40(3):992-1003. [In Chinese].
doi: 10.6038/pg2025HH0590
 21. Liu Q, Wang YX, Xu YG. Synchrosqueezing extracting transform and its application in bearing fault diagnosis under non-stationary conditions. *Measurement.* 2021;173:108569.
doi: 10.1016/j.measurement.2020.108569
 22. Xie QH, Zhao CD, Rui ZF, Guan SJ, Zheng WT, Fan HC. An improved ant-tracking workflow based on divided-frequency data for fracture detection. *J Geophys Eng.* 2022;19(5):1149-1162.
doi: 10.1093/jge/gxac075
 23. Yu C, Wang SY, Cheng LF. Application of high-resolution processing in seismic data based on an improved synchrosqueezing transform. *Front Earth Sci.* 2022;10:956817.
doi: 10.3389/feart.2022.956817
 24. Zhang HX, Wu XF, He BS, Guo M. Time-synchroextracting of generalized S-transform and its application in fault identification. *J Appl Geophys.* 2023;216:105147.
doi: 10.1016/j.jappgeo.2023.105147
 25. Wang Q, Li YX, Chen SJ, Tang B. Matching Demodulation Synchrosqueezing S Transform and its Application in Seismic Time-Frequency Analysis. *IEEE Geosci Remote Sens Lett.* 2022;19:1-5.
doi: 10.1109/LGRS.2020.3047892
 26. Tian L. Seismic spectral decomposition using short-time

- fractional Fourier transform spectrograms. *J Appl Geophys.* 2021;192:104400.
doi: 10.1016/j.jappgeo.2021.104400
27. Chen YP, Peng ZM, Cheng ZY, Tian L. Seismic signal time-frequency analysis based on multi-directional window using greedy strategy. *J Appl Geophys.* 2017;143:116-128.
doi: 10.1016/j.jappgeo.2017.05.017
28. Qin X, Chen S, Zhang S, Li X, Liu Y. The application of frequency-dependent AVO inversion in tight reservoirs area. In: *Proceedings of the SEG Technical Program Expanded Abstracts 2016*. 86th SEG Annual International Meeting; October 21, 2016; Dallas, Texas, USA. Society of Exploration Geophysicists; 2016:3548-3552.
doi: 10.1190/segam2016-13839860.1
29. Yu ZH, Xiao KY, Zhang GL, Xiao GJ, Du YB. Analysis on inverted structure characteristics and its forming mechanism in the Bongor Basin, Chad. *China Pet Explor.* 2018;23(3):90-98. [In Chinese].
doi: 10.3969/j.issn.1672-7703.2018.03.011
30. Li SJ, Wang TY, Gao JH, Liu BY, Gui JY, Wang HQ. lp norm inverse spectral decomposition and its multi-sparsity fusion interpretation. *Appl Geophys.* 2021;18(4):569-578.
doi: 10.1007/s11770-021-0919-x
31. Zheng H, Cai JX, Wang JB. Gaussian beam tomography with structure-filtering and its applications. *Geophys Geochem Explor.* 2020;44(2):372-380. [In Chinese].
doi: 10.11720/wtyh.2020.1300
32. Xie QH, Jiang LW, Zhao CD, Wang ZD, Tang XH, Luo YF. Application study of improving the precision of the ant-tracking-based fracture prediction technique. *Geophys Geochem Explor.* 2021;45(5):1295-1302. [In Chinese].
doi: 10.11720/wtyh.2021.1208